Journal of Mathematical Sciences and Modelling, 4 (3) (2021) 117-125
Research Article

Journal of Mathematical Sciences and Modelling

Journal Homepage: www.dergipark.gov.tr/jmsm
ISSN 2636-8692
DOI: http://dx.doi.org/10.33187/jmsm.1012850

Vortex Solitons on Partially $\mathscr{PT}$-symmetric Azimuthal Lattices in a Medium with Quadratic Nonlinear Response

Mahmut Bağcı[1]

[1]*Department of Software Development, School of Applied Sciences, Yeditepe University, Istanbul, Turkey*

Article Info

Keywords: *Partially Parity-time-symmetric, Quadratic nonlinear media, Vortex solitons*
2010 AMS: *47J35, 35Q55, 81Q05*
Received: *21 October 2021*
Accepted: *16 November 2021*
Available online: *29 December 2021*

Abstract

Vortex solitons in parity-time ($\mathscr{PT}$) symmetric and partially $\mathscr{PT}$ (p$\mathscr{PT}$) symmetric azimuthal lattices are demonstrated for a media with quadratic nonlinear response. Stability properties of the vortices are investigated comprehensively by linear spectra and nonlinear evolution of the governing equations, and it is shown that, although the existence domain of the $\mathscr{PT}$-symmetric and p$\mathscr{PT}$-symmetric lattices are identical, the stability region of $\mathscr{PT}$-symmetric lattice is narrower than that of the p$\mathscr{PT}$-symmetric lattice. It is also observed that deeper real part in the azimuthal potentials supports stability of vortex solitons, whereas deeper imaginary part and strong quadratic electro-optic effects impoverish stability properties of the vortices. Moreover, it is shown that there are different stability properties of vortices in p$\mathscr{PT}$-symmetric azimuthal potentials for different vorticity values, while there is no such difference for vortices in $\mathscr{PT}$-symmetric potentials.

1. Introduction

Solitons are localized waves that arise from a balance between nonlinear and dispersive effects in the medium, and they maintain their shape and velocity during propagation. In the same manner, vortex solitons preserve their angular momentum during propagation. In recent years, there has been considerable attention to soliton dynamics in optically induced lattices (potentials). These external lattices can be perfectly periodic [1, 2], quasi-periodic [3, 4] or irregular structures that possess point or line defects [5].

It is known that if the optical systems include energy gain and loss, the potential of the medium would be complex [6], and such potentials are called parity-time ($\mathscr{PT}$) symmetric. A complex potential $V(x,y)$ is $\mathscr{PT}$-symmetric, if it satisfies the condition $V^*(x,y) = V(-x,-y)$ [6, 7]. In 1998, Bender and Boettcher showed that non-Hermitian Hamiltonians can produce entirely real spectra when they are ($\mathscr{PT}$) symmetric [8], and this fact reveals stable propagation of the solitons in optical systems with $\mathscr{PT}$-symmetric lattices under suitable conditions [9]. $\mathscr{PT}$-symmetric lattices were observed experimentally in [10]-[12] and theoretically in [7], and pulse dynamics in $\mathscr{PT}$-symmetric optical systems are investigated in many studies [13]-[18].

Recently, it has been demonstrated that the spectrum of a complex potential may remain real even if the potential is invariant under complex conjugation and reflection in a single spatial direction (i.e., $V^*(x,y) = V(-x,y)$ or $V^*(x,y) = V(x,-y)$), which means the complex potential is partially $\mathscr{PT}$-symmetric (p$\mathscr{PT}$-symmetric) [19, 20]. Soliton dynamics in such p$\mathscr{PT}$-symmetric lattices have been investigated [20], and symmetry breaking of solitons in p$\mathscr{PT}$-symmetric potentials has been demonstrated by Yang [13, 19]. Symmetry breaking is observed above a critical power, and this power threshold is a bifurcation point after which non-$\mathscr{PT}$-symmetric (asymmetric) solitons can exist. More recently, vortex solitons in p$\mathscr{PT}$-symmetric azimuthal potentials have been introduced in [21], and it is shown that although the considered azimuthal potentials are p$\mathscr{PT}$-symmetric, symmetry breaking of the lattice is not observed. Accordingly, it is shown that stable vortex solitons can be obtained in p$\mathscr{PT}$-symmetric potentials, where the symmetry is already broken in the $\mathscr{PT}$-symmetric counterpart of the potential. The p$\mathscr{PT}$-symmetric azimuthal potentials are constructed from $\mathscr{PT}$-symmetric cells placed on a ring where azimuthal directions (vorticity) become nonequivalent, and the nonequivalence of the azimuthal directions causes remarkable effects on the properties of vortex solitons. Different from vortices in conservative systems, nonequivalent vorticity of the p$\mathscr{PT}$-symmetric potentials causes the disparity of the gain loss distribution along the azimuthal direction. In [21], different internal current distributions have been demonstrated for vortices in such p$\mathscr{PT}$-symmetric azimuthal potentials.

Email addresses and ORCID numbers: bagcimahmut@gmail.com, 0000-0001-6931-6837 (M. Bağcı)

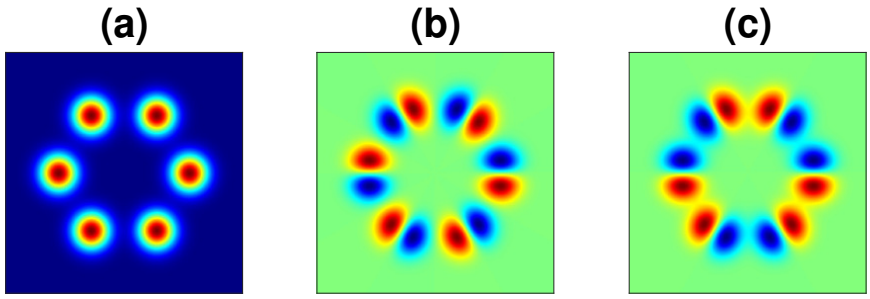

Figure 2.1: Top view of the azimuthal lattices within $(x,y) \in [-4,4]$. (a) Real part V_{re}; (b) Imaginary part (V_{im}) of p$\mathscr{PT}$-symmetric potential when $\sigma = 1$; (c) Imaginary part (V_{im}) of $\mathscr{PT}$-symmetric potential when $\sigma = -1$. The real parts of potentials are identical.

In the abovementioned studies, soliton dynamics of the $\mathscr{PT}$-symmetric and p$\mathscr{PT}$- symmetric lattices have been investigated in cubic nonlinear (Kerr) media that is governed by nonlinear Schrödinger (NLS) type equations. However, it is known that many nonlinear optical systems include materials, such as potassium niobate ($KNbO_3$) [22] or lithium niobate ($LiNbO_3$) [23], that have both cubic and quadratic nonlinear responses [24, 25]. One of the models to describe the nonlinear evolution of the optical waves in quadratically polarized media is the NLS equation with coupling to a mean term (denoted as NLSM systems). The NLSM equations were introduced to characterize water waves by Benney and Roskes in 1969 [26] and extended to three-dimensional wave packets by Davey and Stewartson in 1974 [27], then Ablowitz *et al.* [24, 28, 29] derived an equivalent form of the NLSM model to characterize the pulse dynamics in non-resonant quadratic materials. Recently, the existence of ground-state solution for the NLSM system was demonstrated and collapse dynamics were investigated [30] and it was shown that wave collapse in the NLSM system can be arrested by self-rectification [22]. Latterly, collapse of the NLSM system has been arrested by real periodic [31], quasiperiodic [32] and p$\mathscr{PT}$-symmetric [33] external lattices. The general NLSM system is defined as [22, 28, 29]

$$iu_z + \Delta u + |u|^2 u - \rho u\phi = 0, \qquad \phi_{xx} + \nu\phi_{yy} = \left(|u|^2\right)_{xx}$$

where $u(x,y)$ is the normalized amplitude of the envelope of the normalized static electric field propagating in the z direction. $\Delta u \equiv u_{xx} + u_{yy}$ corresponds to diffraction, and the cubic term in u originates from the nonlinear (Kerr) change of the refractive index. ρ denotes the combined optical rectification and electro-optic effects modeled by the $\phi(x,y)$ field, and ν shows the anisotropy of the material.

These equations come from the interplay between the fundamental and dc fields while the second-harmonic-generation (SHG) is not phase matched. In such circumstances, an additional self-phase modulation contribution is produced by the SHG due to cascaded nonlinearity. Consequently, the NLSM system is a nonlocal nonlinear coupling between the first field and a static field that is emerged from the zeroth harmonic (mean term) [24, 28, 29].

In this study, the numerical existence of vortex solitons in $\mathscr{PT}$-symmetric and p$\mathscr{PT}$-symmetric azimuthal lattices are demonstrated for a medium with quadratic nonlinear response, and stability properties of the obtained vortex solitons are investigated comprehensively by linear spectrum and nonlinear evolution of the governing equations. The model equations are given as the NLSM system with an additional external potential. The paper is outlined as follows: In Sec. 2, the model equations and the azimuthal potentials are presented, and vortex soliton solutions of the model are obtained by numerical methods. In Sec. 3, stability of the vortex solitons are examined by the nonlinear evolution and linear stability spectra of the model, and impact of the vorticity on vortex stability is investigated. Results of the study is summarized in Sec. 4.

2. The Model

Pulse dynamics in a medium with quadratic nonlinear response and an additional external potential is governed by the following (2+1) dimensional model

$$iu_z + \Delta u + |u|^2 u - \rho u\phi + [p_{re}V_{re}(x,y) - ip_{im}V_{im}(x,y)]u = 0, \qquad \phi_{xx} + \nu\phi_{yy} = \left(|u|^2\right)_{xx} \tag{2.1}$$

where p_{re} and p_{im} are the depths of real and imaginary parts of the complex potential $V(x,y)$, respectively. The potential $V(x,y)$ is defined as N Gaussian waveguides that are placed on a ring of radius r_0 [21]:

$$V_{re} = \sum_{k=1}^{N} e^{-[(x-r_0\cos\theta_k)^2+(y-r_0\sin\theta_k)^2]/\alpha^2}$$
$$V_{im} = \sum_{k=1}^{N} \sigma^{k-1}(y\cos\theta_k - x\sin\theta_k)e^{-[(x-r_0\cos\theta_k)^2+(y-r_0\sin\theta_k)^2]/\alpha^2}$$

where $\sigma = \pm 1$, $\theta_k = 2\pi(k-1)/N$ and α is waveguide width. For $\sigma = -1$ the potential is $\mathscr{PT}$-symmetric, i.e., $V(x,y) = V(-x,y) = V^*(x,-y) = V^*(-x,-y)$, and for $\sigma = 1$, it is p$\mathscr{PT}$-symmetric, i.e., $V(x,y) = V^*(-x,y) = V^*(x,-y) \neq V^*(-x,-y)$. We consider $\mathscr{PT}$ and p$\mathscr{PT}$-symmetric azimuthal potentials with $N = 6$, the radius $r_0 = N/2$ and the waveguide width $\alpha = 0.5$. Real and imaginary parts of $\mathscr{PT}$ ($\sigma = -1$) and p$\mathscr{PT}$-symmetric ($\sigma = 1$) azimuthal potentials are displayed in Figure 2.1. The phase transition point was determined as $p_{im} = 7.2$ for $\mathscr{PT}$-symmetric case of the lattice when $p_{re} = 5$ [21]. Above this threshold value, spectrum of the lattice include eigenvalues with non-zero imaginary parts. Phase transition is not observed for the p$\mathscr{PT}$-symmetric azimuthal potential (when $\sigma = 1$).

2.1. Numerical solution for the vortex solitons

The steady state solution (vortex solitons) of the considered model (2.1) is obtained via squared operator method (SOM) that has been developed by Yang [34]. It has been shown that steady state solutions of a wide range of nonlinear wave equations can be computed efficiently by the SOM algorithm. The algorithm is outlined as follows:
Inserting the ansatz $u = U(x,y)\exp(i\mu z)$ into the system (2.1), the operator $\mathbf{L}_0$ is obtained,

$$\mathbf{L}_0\mathbf{u} = -\mu U + \Delta U + |U|^2 U - \rho\phi U + VU, \qquad \phi_{xx} + \nu\phi_{yy} = \left(|U|^2\right)_{xx}$$

where μ is the eigenvalue (propagation constant). Splitting the operator $\mathbf{L}_0$ into its real and imaginary parts and applying Fourier transformation, we get the sub-operators $T1$ and $T2$ as follows:

$$T1 = \mathrm{Re}\left(\mathscr{F}^{-1}\left(\frac{\mathscr{F}(\mathbf{L}_0\mathbf{u})}{K^2+c}\right)\right), \qquad T2 = \mathrm{Im}\left(\mathscr{F}^{-1}\left(\frac{\mathscr{F}(\mathbf{L}_0\mathbf{u})}{K^2+c}\right)\right).$$

where $\mathscr{F}$ denotes Fourier transformation, $k = (k_x, k_y)$ are Fourier variables, $K^2 = k_x^2 + k_y^2$ and c is a real positive number that is chosen heuristically for parametrizing the algorithm. Separating the amplitue U into its real and imaginary parts $U = U_{re}(x,y) + iU_{im}(x,y)$ and substituting into the operator $\mathbf{L}_0\mathbf{u}$ (2.2), we get sub-operators L_{Re} and L_{Im} as follows:

$$L_{\mathrm{Re}} = -\mu U_{re} + \Delta U_{re} + (U_{re}^3 + U_{re}U_{im}^2) - \rho\phi U_{re} + p_{re}V_{re}U_{re} + p_{im}V_{im}U_{im}$$

$$L_{\mathrm{Im}} = -\mu U_{im} + \Delta U_{im} + (U_{im}^3 + U_{re}^2 U_{im}) - \rho\phi U_{im} + p_{re}V_{re}U_{im} - p_{im}V_{im}U_{re}.$$

Taking partial derivatives of L_{Re} and L_{Im} with respect to both U_{re} and U_{im} gives elements of the operator $\mathbf{L}_1$,

$$R_{11} = \frac{\partial L_{\mathrm{Re}}}{\partial U_{re}}(T1), \quad R_{12} = \frac{\partial L_{\mathrm{Re}}}{\partial U_{im}}(T2),$$

$$R_{21} = \frac{\partial L_{\mathrm{Im}}}{\partial U_{re}}(T1), \quad R_{22} = \frac{\partial L_{\mathrm{Im}}}{\partial U_{im}}(T2).$$

and the operator $\mathbf{L}_1$ is defined as

$$\mathbf{L}_1\mathbf{u} = R_{11} + R_{12} + i(R_{21} + R_{22}).$$

After $\mathbf{L}_0$ and $\mathbf{L}_1$ are obtained, the algorithm is iterated as follows,

$$U_{n+1} = U_n - \left(\mathscr{F}^{-1}\left(\frac{\mathscr{F}(\mathbf{L}_1\mathbf{u})}{K^2+c}\right)\right)\Delta t,$$

$$\mu_{n+1} = \mu_n + \|u\cdot T1 + v\cdot T2\|\Delta t,$$

$$\phi_{n+1} = \mathscr{F}^{-1}\left(\frac{k_x^2\mathscr{F}\left(|U_n|^2\right)}{k_x^2+\nu k_y^2}\right).$$

This numerical scheme is implemented until the error

$$E = \sqrt{\|U_{n+1} - U_n\|^2} + |\mu_{n+1} - \mu_n| < 10^{-8},$$

and this algortihm is convergent while the time step Δt is below a certain threshold [34].
To obtain vortex solitons of the model (2.1), the initial condition of the SOM algorithm is chosen as

$$u(x,y,z) = U(\mathbf{r})exp[im\theta(\mathbf{r}) + i\mu z] \tag{2.2}$$

where $\mathbf{r} = (x,y)$, U is field module, θ is the phase, m is vorticity and μ is the propagation constant. The considered azimuthal potentials ($N = 6$) support six-hump vortex solitons for the following parameter set:

$$(\rho, \nu, p_{re}, p_{im}, \mu, m) = (0.5, 1.5, 6, 1, 0.5, 1). \tag{2.3}$$

It is noted that $\rho = 0.5$ and $\nu = 1.5$ are particularly selected parameter values to characterize quadratic electro-optic effects in potassium niobate ($KNbO_3$) [22].
In Figure 2.2, the vortex profile, the top view and the phase structure are shown for the azimuthal potentials when $\sigma = 1$ (p$\mathscr{P}\mathscr{T}$-symmetric) in the first row (a) and when $\sigma = -1$ ($\mathscr{P}\mathscr{T}$-symmetric) in the second row (b). It can be seen that there are six-hump vortex structures that are located at local maxima of the considered azimuthal potentials.

3. Power and Stability Analysis

The vortex solutions of the model (2.1) is computed by the SOM algorithm, and the stability dynamics of these vortex solitons are studied by the linear stability spectra and nonlinear evolution of the model.

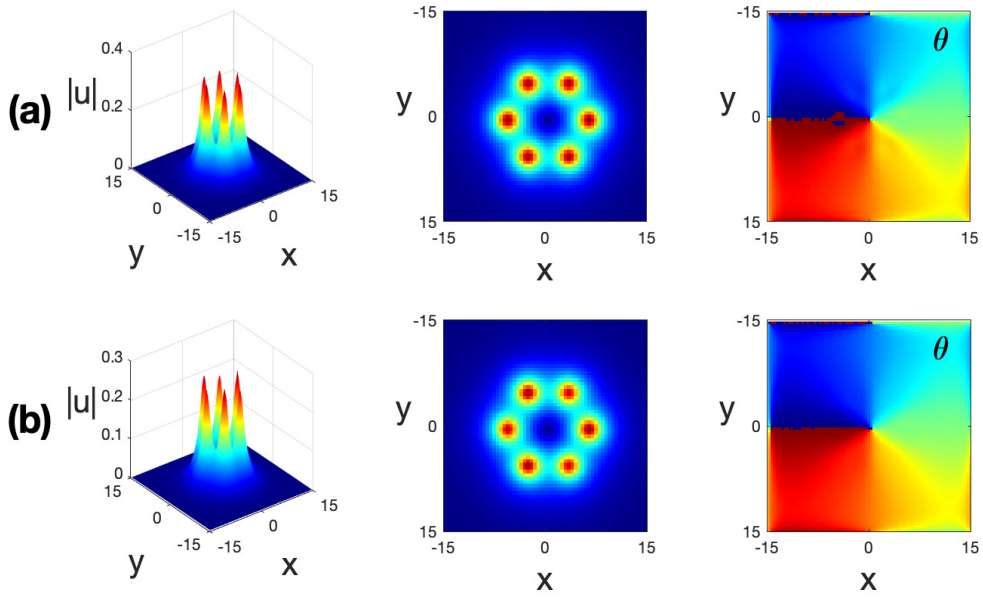

Figure 2.2: 3D profile, top view and phase structure of the six-hump vortex solitons located at local maxima of the azimuthal potential for the parameters given in (2.3) (a) when $\sigma = 1$ (the first row); (b) when $\sigma = -1$ (the second row). $c = 2$, $\Delta t = 0.2$ and vorticity $m = 1$ in both cases.

3.1. Linear stability analysis

The model (2.1) is linearized to calculate linear spectrum of vortex solitons as follows. By denoting

$$U = e^{i\mu z}[u_0(x,y) + g(x,y)e^{\lambda z} + h^*(x,y)e^{\lambda^* z}]$$

where $u_0(x,y)$ is the vortex soliton and $g,h \ll 1$ are perturbed infinitesimal modes. Inserting the perturbed solution U into the model (2.1), the following eigenvalue problem is obtained

$$\mathscr{L}\mathbf{V} = \lambda\mathbf{V}$$

where

$$\mathscr{L} = i\begin{pmatrix} \mathscr{L}_{11} & \mathscr{L}_{12} \\ \mathscr{L}_{21} & \mathscr{L}_{22} \end{pmatrix}, \quad \mathbf{V} = \begin{pmatrix} g \\ h \end{pmatrix}$$

and the matrix coefficients of $\mathscr{L}$ are

$$\begin{aligned} \mathscr{L}_{11} &= \Delta - \mu - \rho\phi + V, \\ \mathscr{L}_{12} &= u^2, \\ \mathscr{L}_{21} &= -(u^2)^*, \\ \mathscr{L}_{22} &= -(\Delta - \mu - \rho\phi + V)^*. \end{aligned}$$

The eigenvalues of $\mathscr{L}$ can be calculated numerically by the Fourier collocation method [35]. If any eigenvalue in the spectrum has a positive real part, the solution is linearly unstable.

The power of solitons, that is calculated by P=$\iint_{-\infty}^{\infty} |u|^2 dxdy$, plays an important role in the stability analysis. Therefore, the power-eigenvalue diagram of gap solitons are investigated in Figure 3.1(a), and stability properties of considered vortex solitons are investigated in Figure 3.1(b) for the same parameters. Blue line shows p$\mathscr{PT}$-symmetric ($\sigma = 1$) and red line shows $\mathscr{PT}$-symmetric ($\sigma = -1$) case of the azimuthal potential. In Figure 3.1(a), the linear stability (solid line) and instability (dotted) regions are determined by computation of eigenvalue spectra for each point on the power curves and the maximum real parts of these spectra are given in Figure 3.1(b). From the power-eigenvalue ($P - \mu$) diagram, it can be seen that the vortices are linearly stable below a critical power $P_c = 4.14$, that corresponds to $\mu = 0.58$, in both $\sigma = 1$ and $\sigma = -1$ cases when $p_{re} = 6$ and $p_{im} = 1$ (see Figure 3.1(a)).

Similarly, the power and stability properties of vortex solitons are shown in Figure 3.2 for the parameters ρ, ν, p_{re} and p_{im}. It is important to note that this analysis shows the first band-gap boundaries for the considered parameter regimes in each panel. For instance, when $\nu = 1.5$, $p_{re} = 6$, $p_{im} = 1$, $\mu = 0.5$ and $\sigma = 1$, the vortex solitons can be obtained for $\rho \in [0, 1.85]$ within the gap region (see blue line in Figure 3.2(a)). It is observed that, although linear stability region for the anisotropy coefficient ν and potential depth of real part p_{re} are identical in both $\sigma = 1$ and $\sigma = -1$ cases, stability region of p$\mathscr{PT}$-symmetric ($\sigma = 1$) lattice is larger than that of $\mathscr{PT}$-symmetric ($\sigma = -1$) lattice for the coupling parameter ρ and potential depth of imaginary part p_{im}.

The vortex solitons that are shown in Figure 2.2(a) and 2.2(b) correspond to 'a' and 'b' points in Figure 3.2(d), respectively. This fact reveals the linear stability of the vortices at point 'a' and 'b' when $\sigma = 1$ and $\sigma = -1$.

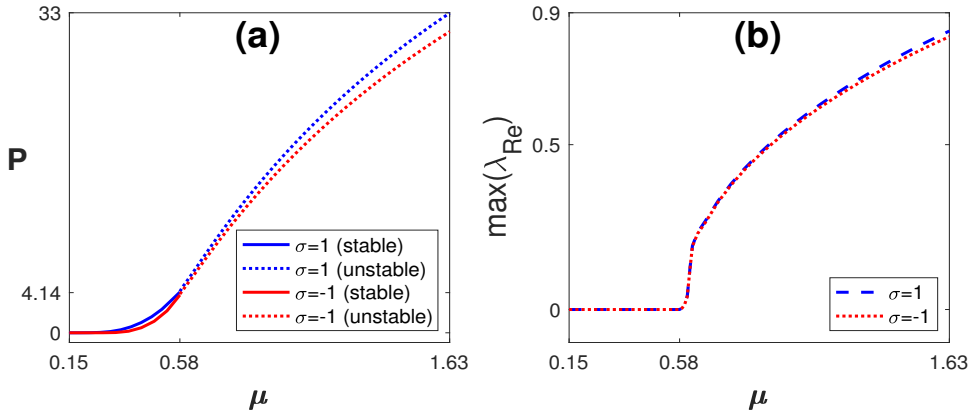

Figure 3.1: The power of vortex solitons versus eigenvalue (a) and the maximum real part in the eigenvalue spectrum (b) for varied values of μ when $\rho = 0.5$, $\nu = 1.5$, $p_{re} = 6$ and $p_{im} = 1$.

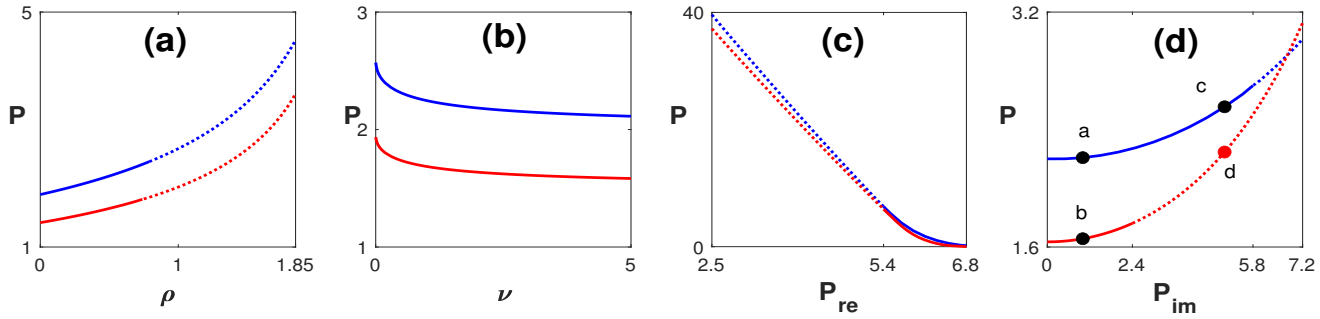

Figure 3.2: The power of vortex solitons (a) for varied values of ρ when $\nu = 1.5$, $p_{re} = 6$, $p_{im} = 1$ and $\mu = 0.5$; (b) for varied values of ν when $\rho = 0.5$, $p_{re} = 6$, $p_{im} = 1$ and $\mu = 0.5$; (c) for varied values of p_{re} when $\rho = 0.5$, $\nu = 1.5$, $p_{im} = 1$ and $\mu = 0.5$; (d) for varied values of p_{im} when $\rho = 0.5$, $\nu = 1.5$, $p_{re} = 6$ and $\mu = 0.5$. Blue line shows p$\mathscr{P}\mathscr{T}$-symmetric ($\sigma = 1$) and red line shows $\mathscr{P}\mathscr{T}$-symmetric ($\sigma = -1$) case of the azimuthal potential where solid and dotted line show stable and unstable regions for the gap solitons, respectively.

3.2. Nonlinear evolution of vortex solitons

To test the full stability, the nonlinear stability of vortex solitons are investigated by direct simulation of the model (2.1) for long times. A finite-difference discretization scheme is used in the spatial domain and the solution is advanced in z with a fourth-order Runge-Kutta method. The initial condition of evolution is taken to be a vortex structure that is obtained by the SOM algorithm and perturbed with 1% random noise in amplitude and phase.

Linear stability spectra and nonlinear evolution of the vortices, that are obtained at 'a', 'b', 'c' and 'd' points in Figure 3.2(d), are examined in columns (a), (b), (c) and (d) of Figure 3.3, respectively. The nonlinear evolution of perturbed vortices (the first row), linear stability spectra (the second row) and 3D view of the evolved vortex profiles (the third row) are shown in Figure 3.3. As can be seen from Figure 3.3(a), 3.3(b) and 3.3(c), the linear spectra of vortex solitons that are obtained at 'a', 'b', 'c' points are purely-imaginary (none of their eigenvalues have a real part), the peak amplitude of the evolved vortices oscillate relatively small amplitudes during the propagation, and vortex profiles are preserved after evolution at $z = 500$, thus stable evolution of the vortex structures can be achieved for the considered parameter regimes. On the other hand, the linear spectrum of the vortex solitons, that is obtained at point 'd', involves eigenvalues with positive real parts, peak amplitude of the evolved soliton increases significantly during the evolution and the vortex profile breaks up after evolution at $z = 500$ (see Figure 3.3(d)). These facts indicate the instability of vortex structure due to blow-up of solitons when $\sigma = -1, p_{re} = 6$ and $p_{im} = 5$.

It should be noted that the result of nonlinear evolution analysis is consistent with linear (in)stability regions that are given in Figure 3.2 for the $\mathscr{P}\mathscr{T}$-symmetric and p$\mathscr{P}\mathscr{T}$-symmetric azimuthal lattices. To see the impact of quadratic optical effects and depth of p$\mathscr{P}\mathscr{T}$-symmetric azimuthal lattices on the pulse stability, the evolution of peak amplitudes are examined for varied ρ, ν, p_{re} and p_{im} values in Figure 3.4. Here, the initial condition is chosen as the vortex at point 'd' that is shown to be nonlinearly unstable in Figure 3.3(d), and the initial peak amplitude of the vortex solitons are normalized to 1 for comparison. The results in Figure 3.4 show that, by increasing the value of optical rectification parameter ρ and lattice depth of the imaginary part p_{im}, peak amplitude of vortices are increasing more rapidly, and thus collapse of vortices are accelerated (see panels (a) and (d)). Conversely, the increase in peak amplitude can be delayed by increasing anisotropy parameter ν and lattice depth of the real part p_{re} (see panels (b) and (c)). These results consistent with previous studies that have demonstrated stability of two dimensional solitons that are generated by the NLSM system with periodic [31], quasi-periodic [32] and p$\mathscr{P}\mathscr{T}$-symmetric [33] lattices. In [31], it was also shown that, collapse will eventually occur in a lattice-free NLSM system, and collapse of the solitons are expedited by increasing values of ρ and ν in the lattice-free medium.

It should be noted that, although vortex solitons can be obtained in semi-infinite interval when $\nu > 0$ and increased values of ν assists maintaining the peak amplitude of the vortices in the p$\mathscr{P}\mathscr{T}$-symmetric azimuthal lattices, it can not be considered as a collapse arrest mechanism, since ρ and ν parameters are prescribed coefficients that are depending on the type of optical materials.

In addition, it is observed that, as shown in [21], there is different stability properties of vortices for different vorticity values that is denoted by m in equation (2.2) and fixed to 1 in the study. Linear stability spectra and peak amplitudes of the evolved vortices are displayed in Figure 3.5 for $m = +1$ and $m = -1$ when $\rho = 1, \nu = 1.5, p_{re} = 6, p_{im} = 1$ and $\mu = 1$. As can be seen from Figure 3.5, although the linear stability spectra and nonlinear evolution of the vortices are overlapping for the $\mathscr{P}\mathscr{T}$-symmetric lattice ($\sigma = -1$) (see the second row (b)),

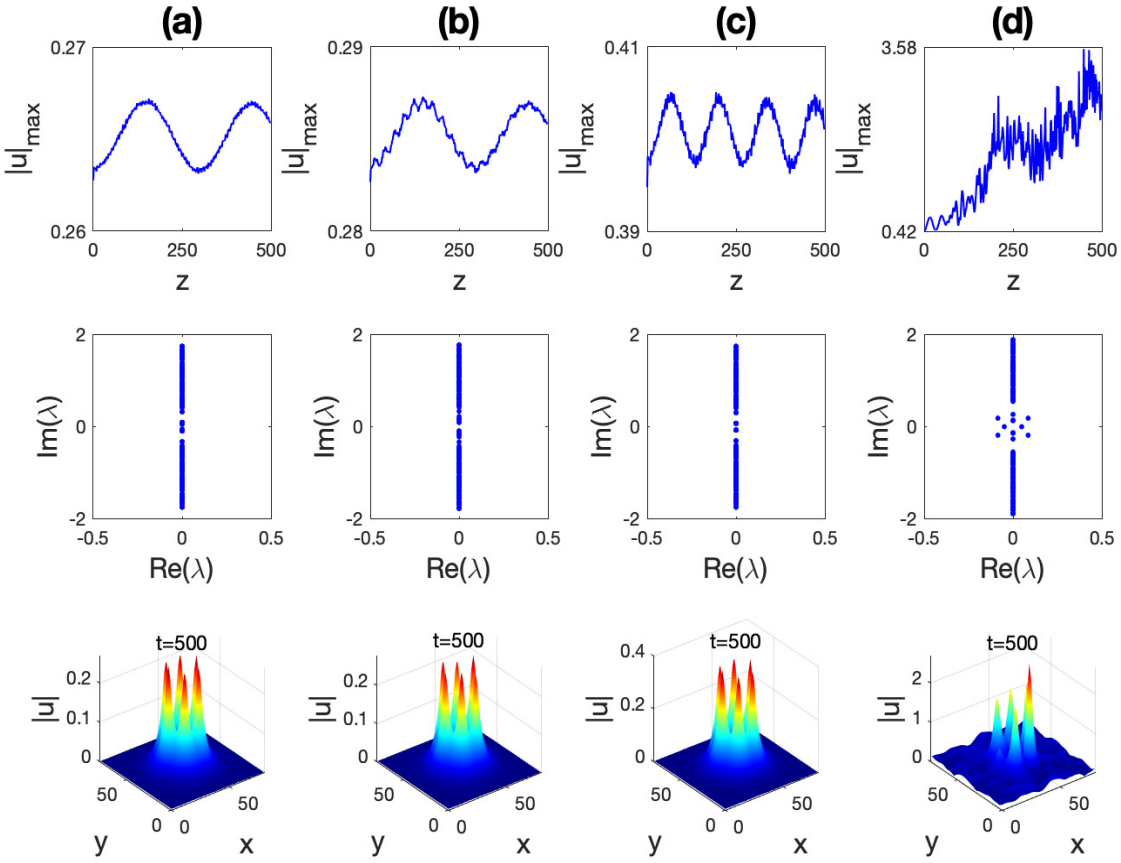

Figure 3.3: The peak amplitude of evolved vortices from $z = 0$ to $z = 500$ (the first row), linear stability spectra (the second row) and 3D view of vortex profile after evolution at $z = 500$ (the third row). The vortex solitons are generated (a) when $\sigma = 1$, $p_{re} = 6$ and $p_{im} = 1$; (b) when $\sigma = -1$, $p_{re} = 6$ and $p_{im} = 1$; (c) when $\sigma = 1$, $p_{re} = 6$ and $p_{im} = 5$; (d) when $\sigma = -1$, $p_{re} = 6$ and $p_{im} = 5$. $\rho = 0.5$, $\nu = 1.5$ and $\mu = 0.5$ in all cases.

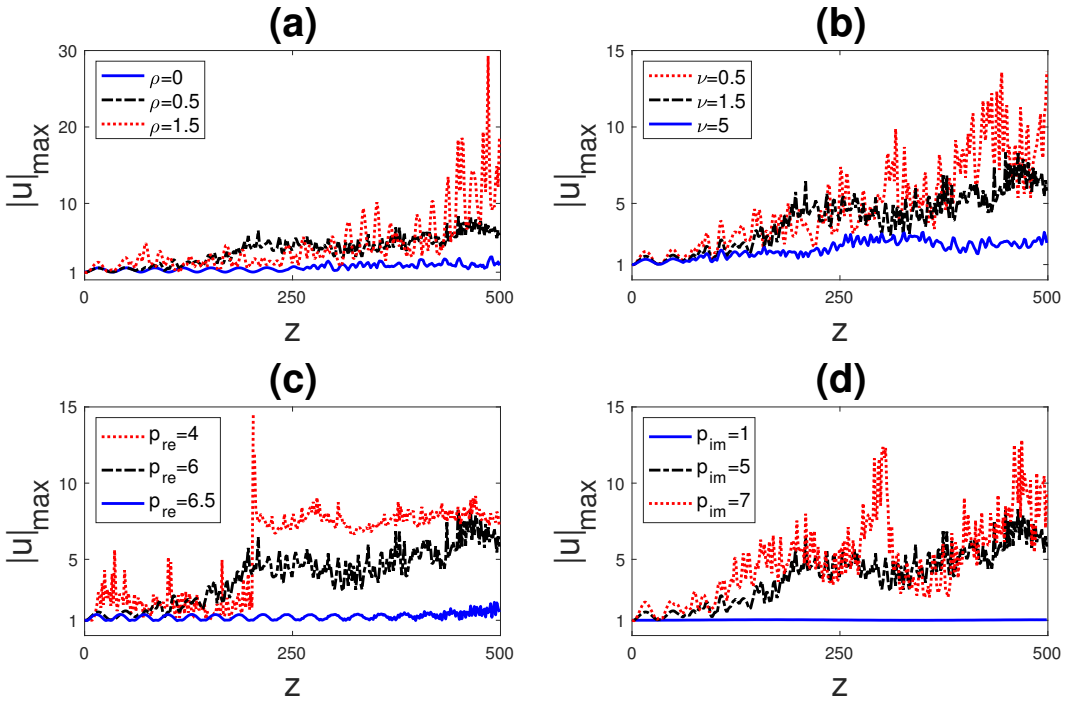

Figure 3.4: The peak amplitude of the evolved vortices in the p$\mathscr{P}\mathscr{T}$-symmetric azimuthal potential. The vortex is obtained (a) for varied values of ρ when $\nu = 1.5$, $p_{re} = 6$ and $p_{im} = 5$; (b) for varied values of ν when $\rho = 0.5$, $p_{re} = 6$ and $p_{im} = 5$; (c) for varied values of p_{re} when $\rho = 0.5, \nu = 1.5$ and $p_{im} = 5$; and (d) for varied values of p_{im} when when $\rho = 0.5, \nu = 1.5$ and $p_{re} = 6$. $\mu = 0.5$ in all cases.

the stability spectra and nonlinear evolution of the vortices are different for the p$\mathscr{P}\mathscr{T}$-symmetric lattice ($\sigma = 1$) (see the first row (a)). The maximum real part in the linear stability spectrum for $m = +1$ is larger than that for $m = -1$ when $\sigma = -1$ (see left panel in Figure 3.5(a)).

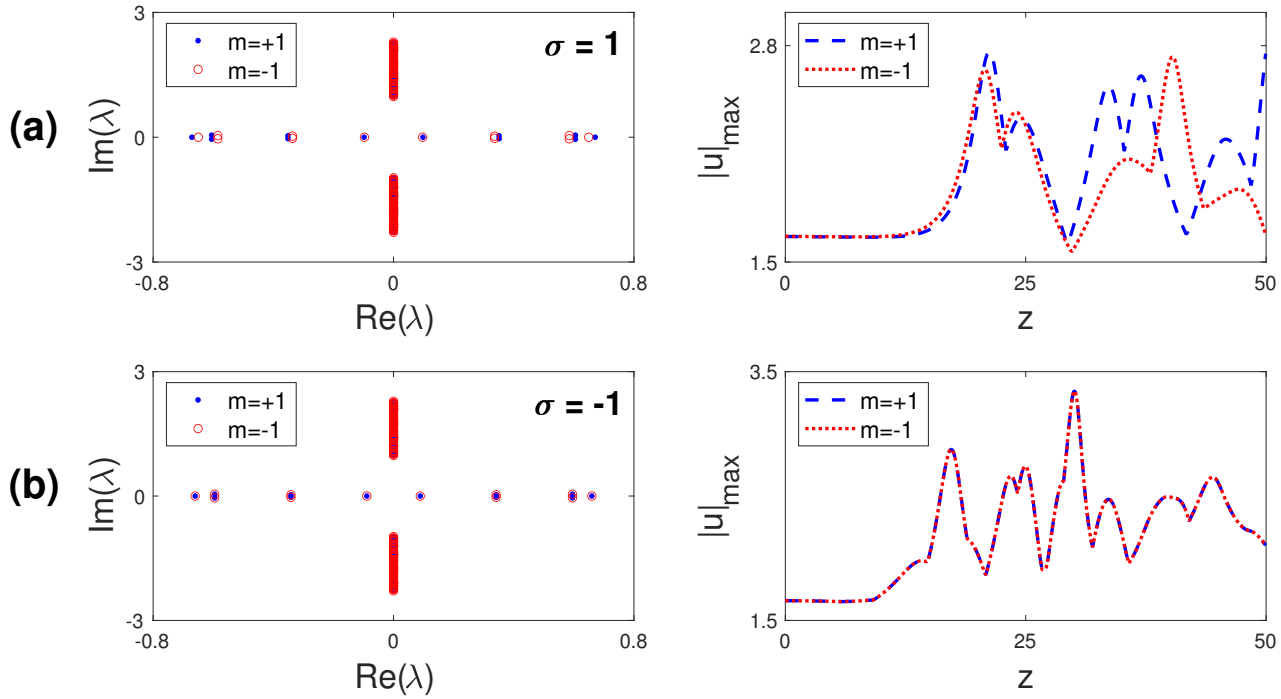

Figure 3.5: The linear stability spectra (the first column) and peak amplitude of evolved vortices from $z = 0$ to $z = 50$ (the second column) for $m = +1$ and $m = -1$. The vortex solitons are generated when $\rho = 1, \nu = 1.5, p_{re} = 6, p_{im} = 1$ and $\mu = 1$ (a) for the p$\mathscr{P}\mathscr{T}$-symmetric lattice ($\sigma = 1$); (b) for the $\mathscr{P}\mathscr{T}$-symmetric lattice ($\sigma = -1$)

In order to support this result, the maximum real part in the spectrum versus eigenvalue(μ) is depicted in Figure 3.6 for $m = +1$ and $m = -1$. It is shown that the difference between the maximum real parts in the spectra are increasing with increasing values of μ for the examined

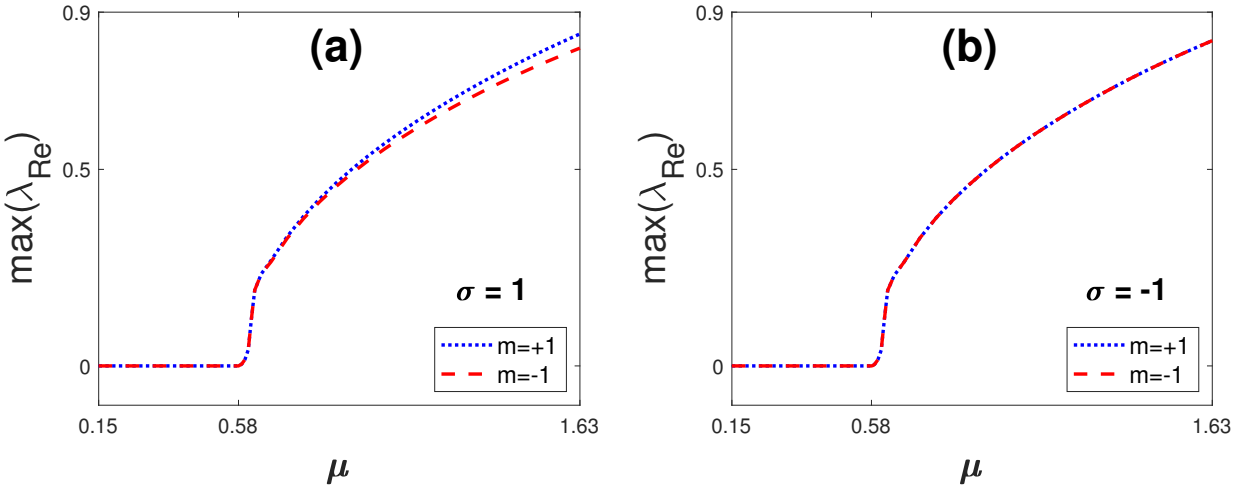

Figure 3.6: The maximum real part in the spectrum versus propagation constant (μ) for $m = +1$ and $m = -1$ (a) when $\sigma = 1$; (b) when $\sigma = -1$. $\rho = 0.5$, $\nu = 1.5$, $p_{re} = 6$ and $p_{im} = 1$ in all cases.

vorticity values ($m = +1$ and $m = -1$) in the p$\mathscr{P}\mathscr{T}$-symmetric lattice (see panel (a)). In contrast, no such difference is observed in the $\mathscr{P}\mathscr{T}$-symmetric lattice for different vorticity values (see panel (b)).

4. Conclusions

The numerical existence of vortex solitons in $\mathscr{P}\mathscr{T}$-symmetric ($\sigma = -1$) and p$\mathscr{P}\mathscr{T}$-symmetric ($\sigma = 1$) azimuthal potentials are demonstrated for the quadratic nonlinear media, and stability properties in the considered lattices are explored by examining the nonlinear evolution and linear stability spectra of the vortex structures. It has been shown that, although the existence domain of the $\mathscr{P}\mathscr{T}$-symmetric and p$\mathscr{P}\mathscr{T}$-symmetric lattices are identical, the stability region of $\mathscr{P}\mathscr{T}$-symmetric lattice is narrower than that of the p$\mathscr{P}\mathscr{T}$-symmetric lattice. Linear stability spectra and nonlinear evolution of vortices show that, the stable evolution of vortex structures can be achieved in both $\mathscr{P}\mathscr{T}$-symmetric and p$\mathscr{P}\mathscr{T}$-symmetric azimuthal potentials for a wide range of parameters, and although there is a threshold value of the depth of imaginary part in the $\mathscr{P}\mathscr{T}$-symmetric potential for the stability of vortices, there is not any phase-transition point for the

p$\mathscr{P}\mathscr{T}$-symmetric potential. Accordingly, it is demonstrated that stable vortex structures can exist in p$\mathscr{P}\mathscr{T}$-symmetric potentials, where the symmetry is already broken in the $\mathscr{P}\mathscr{T}$-symmetric counterpart of the potential.
Moreover, it has been observed that there are different stability properties of vortices in p$\mathscr{P}\mathscr{T}$-symmetric azimuthal potentials for different vorticity values, while there is no such difference for vortices in $\mathscr{P}\mathscr{T}$-symmetric potentials.
Linear stability spectra together with the nonlinear evolution reveal that deeper real part in the azimuthal potentials support stability of vortices, whereas deeper imaginary part and strong quadratic electro-optic effects in the medium impoverish stability properties of the vortices.

Acknowledgements

The authors would like to express their sincere thanks to the editor and the anonymous reviewers for their helpful comments and suggestions.

Funding

There is no funding for this work.

Availability of data and materials

Not applicable.

Competing interests

The authors declare that they have no competing interests.

Authors' contributions

All authors contributed equally to the writing of this paper. All authors read and approved the final manuscript.

References

[1] M. J. Ablowitz, N. Antar, İ. Bakırtaş, B. Ilan, *Band-gap boundaries and fundamental solitons in complex two-dimensional nonlinear lattices*, Phys. Rev. A., **81**(3) (2010), 033834.
[2] M. J. Ablowitz, N. Antar, İ. Bakırtaş, B. Ilan, *Vortex and dipole solitons in complex two-dimensional nonlinear lattices*, Phys. Rev. A., **86**(3) (2012), 033804.
[3] M. J. Ablowitz, B. Ilan, E. Schonbrun, R. Piestun, *Solitons in two-dimensional lattices possessing defects, dislocations, and quasicrystal structures*, Phys. Rev. E., **74**(3) (2006), 035601.
[4] G. Burlak, B. A. Malomed, *Matter-wave solitons with the minimum number of particles in two-dimensional quasiperiodic potentials*, Phys. Rev. E., **85**(5) (2012), 057601.
[5] M. Bağcı, İ. Bakırtaş, N. Antar, *Vortex and dipole solitons in lattices possessing defects and dislocations*, Opt. Commun., **331** (2014), 204-218.
[6] J. Yang, *Necessity of pt symmetry for soliton families in one-dimensional complex potentials*, Phys. Lett. A., **378**(4) (2014), 367-373.
[7] D. N. Christodoulides, J. Yang, *Parity-Time Symmetry and Its Applications*, Singapore, Springer, 2018.
[8] C. M. Bender, S. Boettcher, *Real spectra in non-hermitian hamiltonians having PT symmetry*, Phys. Rev. Lett., **80**(24) (1998), 5243-5246.
[9] K. G. Makris, R. El-Ganainy, D. N. Christodoulides, Z. H. Musslimani, *Beam dynamics in PT symmetric optical lattices*, Phys. Rev. Lett., **100**(10) (2008), 103904.
[10] C. E. Rüter, K. G. Makris, R. El-Ganainy, D. N. Christodoulides, M. Segev, D. Kip, *Observation of parity-time symmetry in optics*, Nat. Phys., **6**(3) (2010), 192-195.
[11] A. Regensburger, C. Bersch, M. A. Miri, G. Onishchukov, D. N. Christodoulides, U. Peschel, *Parity-time synthetic photonic lattices*, Nature, **488** (2012), 167-171.
[12] L. Feng, R. El-Ganainy, L. Ge, *Non-hermitian photonics based on parity-time symmetry*, Nat. Photon, **11**(12) (2017), 752-762.
[13] J. Yang, *Symmetry breaking of solitons in one-dimensional parity-time-symmetric optical potentials*, Opt. Lett., **39**(19) (2014), 5547-5550.
[14] İ. Göksel, N. Antar, İ. Bakırtaş, *Solitons of (1+1)d cubic-quintic nonlinear Schrödinger equation with pt-symmetric potentials*, Opt. Commun., **354** (2015), 277-285.
[15] Q. Zhou,, A. Biswas, *Optical solitons in parity-time-symmetric mixed linear and nonlinear lattice with non-Kerr law nonlinearity*, Superlattices and Microstructures, **109** (2017), 588-598.
[16] M. Bağcı, İ. Bakırtaş, N. Antar, *Fundamental solitons in parity-time symmetric lattice with a vacancy defect*, Opt. Commun., **356** (2015), 472-481.
[17] İ. Göksel, N. Antar, İ. Bakırtaş, *Two-dimensional solitons in PT-symmetric optical media with competing nonlinearity*, Optik., **156** (2018), 470-478.
[18] İ. Göksel, N. Antar, İ. Bakırtaş, *Two-dimensional solitons in cubic-saturable media with PT-symmetric lattices*, Chaos Solitons Fractals., **109** (2018), 83-89
[19] J. Yang, *Symmetry breaking of solitons in two-dimensional complex potentials*, Phys. Rev. E., **91**(2) (2015), 023201.
[20] J. Yang, *Partially PT symmetric optical potentials with all-real spectra and soliton families in multidimensions*, Opt. Lett., **39**(5) (2014), 1133-1136.
[21] Y. V. Kartashov, V. V. Konotop, L. Torner, *Topological states in partially-PT -symmetric azimuthal potentials*, Phys. Rev. Lett., **115**(19) (2015), 193902.
[22] L. C. Crasovan, J. P. Torres, D. Mihalache, L. Torner, *Arresting wave collapse by wave self- rectification*, Phys. Rev. Lett., **91**(6) (2003), 063904.
[23] R. Schiek, T. Pertsch,*Absolute measurement of the quadratic nonlinear susceptibility of lithium niobate in waveguides*, Opt. Mater. Express., **2**(2) (2012), 126-139.
[24] M. J. Ablowitz, G. Biondini, S. Blair, *Localized multi-dimensional optical pulses in non-resonant quadratic materials*, Math. Comput. Simul., **56** (2001), 511-519.
[25] M. Bağcı, J. N. Kutz, *Spatiotemporal mode locking in quadratic nonlinear media*, Phys. Rev. E., **102**(2) (2020), 022205.
[26] D. J. Benney, G. J. Roskes, *Wave instabilities*, Stud. in App. Math., **48** (1969), 377-385.
[27] A. Davey, K. Stewartson, *On three-dimensional packets of surface waves*, Proc. of the Royal Soc. of London. Series A, Math. and Phys. Sci., **338** (1974), 101-110.
[28] M. J. Ablowitz, G. Biondini, S. Blair, *Multi- dimensional pulse propagation in non-resonant $\chi^{(2)}$ materials*, Phys.Lett. A., **236**(5) (1997), 520-524.
[29] M. J. Ablowitz, G. Biondini, S. Blair, *Nonlinear Schrödinger equations with mean terms in nonresonant multidimensional quadratic materials*, Phys. Rev. E., **63**(4) (2001), 046605.
[30] M. J. Ablowitz, İ. Bakırtaş, B. Ilan, *Wave collapse in a class of nonlocal nonlinear Schrödinger equations*, Physica D: Nonlinear Phenomena, **207**(3) (2005), 230-253.
[31] M. Bağcı, İ. Bakırtaş, N. Antar, *Lattice solitons in nonlinear Schrödinger equation with coupling-to-a-mean-term*, Opt. Commun., **383** (2017), 330-340.

[32] M. Bağcı, *Soliton dynamics in quadratic nonlinear media with two-dimensional pythagorean aperiodic lattices*, J. Opt. Soc. Am. B., **38**(4) (2021), 1276-1282.
[33] M. Bağcı, *Partially PT -symmetric lattice solitons in quadratic nonlinear media*, Phys. Rev. A., **103**(2) (2021), 023530.
[34] J. Yang, T. I. Lakoba, *Universally-convergent squared-operator iteration methods for solitary waves in general nonlinear wave equations*, Stud. in App. Math., **118**(2) (2007), 153-197.
[35] J. Yang, *Nonlinear Waves in Integrable and Nonintegrable Systems*, SIAM, Philadelphia, 2010.